



Article

Coating Mechanism of AuNPs onto Sepiolite by Experimental Research and MD Simulation

Deniz Karataş¹ , Dilek Senol Arslan² , Ilgin Kursun Unver² and Orhan Ozdemir^{2,*}

¹ Mineral Processing Engineering Department, Istanbul Technical University, Maslak, 34469 Istanbul, Turkey; karatasde@itu.edu.tr

² Mining Engineering Department, Istanbul University-Cerrahpasa, Avcılar, 34320 Istanbul, Turkey; dilek.senol@istanbul.edu.tr (D.S.A.); ilginkur@istanbul.edu.tr (I.K.U.)

* Correspondence: orhanozdemir@istanbul.edu.tr

Received: 16 October 2019; Accepted: 19 November 2019; Published: 22 November 2019



Abstract: The amenability of gold nanoparticles (AuNPs) coating on natural and modified (hexadecyl trimethyl ammonium bromide, CTAB) sepiolite surfaces was studied both experimentally and theoretically. The zeta potential experiments and Fourier transform infrared spectrophotometer (FTIR), environmental scanning electron microscope (ESEM), and transmission electron microscopy (TEM) analyses were carried out with the sepiolite samples in the presence of AuNPs. In addition, the adsorption of three gold-nanoparticles on the sepiolite surface (100) in the absence and presence of CTAB was investigated by molecular dynamics (MD) simulations. The AuNPs showed no significant change in the zeta potential of natural sepiolite surfaces due to negative charges of both the sepiolite and AuNPs at natural pH. The surface charge of modified sepiolite decreased with the increase in AuNPs concentration indicating the significance AuNPs adsorption. FTIR, ESEM, and TEM analyses indicated the coating of AuNPs onto the modified sepiolite surface were higher than that of the natural sepiolite surface. The MD simulation results showed that AuNPs can easily adsorb onto the basal surface of the sepiolite due to its hydrophilicity in the presence and absence of CTAB as indicated in the experimental studies. In short, the modification of sepiolite with CTAB made the charge positive, and in turn considerably increased the AuNPs coating on sepiolite surfaces due to electrostatic attraction.

Keywords: gold nanoparticles; AuNPs; sepiolite; zeta potential; coating; molecular dynamics simulation; coulomb and van der Waals interactions; H-bonds

1. Introduction

Gold nanoparticles (AuNPs), due to their optical properties, have attracted the interest of many researchers and are widely used in many applications such as electronics, photodynamic therapy, sensors, probes, diagnostics catalysis, cosmetics, nanomedicine, etc. [1–5]. AuNPs are a suspension of submicron gold particles typically dispersed in water, and the color of the suspension changes from red to other colors including brown, yellow, and purple as the particle size changes [6]. Moreover, their optical response may change depending on the particle size, shape, and concentration [7]. Sepiolite (SEP) with the chemical formula of $\text{Mg}_4\text{Si}_6\text{O}_{15}(\text{OH})_2 \cdot 6(\text{H}_2\text{O})$ is a hydrated magnesium silicate with micro and mesoporous structure. Its fiber morphology and the presence of alternating blocks and tunnels that grow in the fiber direction make it an ideal material for use in particular applications such as viscosity, color, plasticity, dry and fired strength, absorption and adsorption, abrasion, and others [8–12].

In recent years, many studies have been conducted experimentally on the adsorption of gold nanoparticles onto clay minerals such as montmorillonite [5,13–16], kaolinite [17], halloysite [18], zeolite [19], and sepiolite [2,5,20–22]. In these studies, it was emphasized that the modification had a

great role in the deposition of AuNPs on the clay surface, and that especially the positively charged salts were important in the coating. For example, in a study, a new nanoparticle was produced by preparing a sepiolite matrix with non-agglomerated and monodisperse metallic nanoparticles. Moreover, it has been proposed that sepiolite can be used in everyday life in optoelectronic applications, forming a pair compatible with gold, one of the metallic nanoparticles [21]. In another study that was conducted about ten years ago, gold nanoparticles produced by supporting with both montmorillonite and sepiolite minerals were mentioned. In a recent study, the adsorption of highly dispersed nanogold particles on purified montmorillonite and sepiolite and functionalized sepiolite samples was investigated. As a result of the characterization tests, it was found that loading of AuNPs onto all three samples took place and the size of AuNPs in the functionalized sepiolite sample was reported as 2.7 nm [5]. In another study, gold nanoparticles were deposited on the outer surfaces of the sepiolite functionalized with aminopropyltriethoxysilane. As a result of the characterization analysis, it was concluded that AuNPs deposited in sepiolite fibers were obtained in very small size and very well dispersed at 2–3 nm and even 100% of AuNPs were below 5 nm and 91% were 3 nm [20]. On the other hand, a number of theoretical studies with both density functional theory (DFT) and molecular dynamics (MD) simulations on the sepiolite mineral have been encountered recently [23–25]. It was revealed in those studies that sepiolite has a mineral structure suitable for both nanoparticles such as silver, platinum, and polymeric nanocomposites. However, the AuNPs/SEP model, which is frequently studied experimentally, has not been hardly encountered in theory. Therefore, in the presence of AuNPs, adsorption and coating on mineral surfaces has become theoretically needed modeling. In this study, adsorption and coating of AuNPs to the basal surface of the sepiolite in the absence/presence of hexadecyltrimethylammonium bromide (CTAB) was experimentally investigated and supported with molecular dynamics (MD) simulations. Here, CTAB has been chosen for its successful modification performance with sepiolite [11,26,27] and also because it is often handled with gold in experimental and theoretical studies [28–32]. Therefore the aim of this study is to reveal the intermolecular interaction of experimentally produced gold nanoparticle loaded sepiolite. In addition, nanoparticles are thought to have potential with suitable properties to be used for optical and magnetic applications.

2. Materials and Methods

2.1. Experimental Studies

The natural sepiolite sample used as an adsorbent in this study was obtained from Sivrihisar region of Turkey. The particle size distribution of sepiolite was also measured using a Malvern Mastersizer 2000 (Malvern Instruments Ltd., Malvern, UK). The sample was first ground to less than 63 μm ($d_{50} \cong 7 \mu\text{m}$) for zeta potential experiments. Complete chemical analysis of the sepiolite is given in Table 1. Additionally, the X-ray diffraction and the chemical analysis indicated that calcite and dolomite were the major impurities in sepiolite sample. A quaternary amine, hexadecyltrimethylammonium bromide (CTAB, $\text{C}_{19}\text{H}_{42}\text{BrN}$), was used for modifying the surface of sepiolite, was purchased from SIGMA, Saint Louis, MO, USA, and specified to be of 99% purity with a molecular weight of 346.46 g/mol. The AuNPs were produced in two samples, 1 and 25 ppm, using the procedure of Frens [33]. The procedure briefly involves mixing of 5% solids with $2 \times 10^{-2} \text{ kmol/m}^3$ CTAB followed by conditioning, solid-liquid separation, and drying [34]. The pH was adjusted by HCl and NaOH. De-ionized (DI) water (18 M Ω ·cm) freshly purified using a setup consisting of a reverse osmosis RO's unit and an Ultrapure Academic Milli-Q system (Millipore Ltd., Molsheim, France) was used for all studies.

Table 1. Chemical composition of sepiolite.

Compound	SiO ₂	Al ₂ O ₃	Fe ₂ O ₃	MgO	CaO	K ₂ O	TiO ₂	P ₂ O ₅	MnO	LOI
%	44.42	2.36	0.95	19.87	2.00	0.33	0.13	0.01	0.01	29.76

2.2. Zeta Potential Measurements

The electrokinetic properties of AuNPs and sepiolite were determined by Brookhaven Zeta Plus equipment (Brookhaven Instruments Corporation, New York, NY, USA). The unit automatically calculates the electrophoretic mobility of particles and then converts it to the zeta potential using the Smoluchowski equation. 0.1 g of natural and modified sepiolites were conditioned in 100 mL of distilled water for 15 min. The pH of suspension was adjusted using 0.1 M HCl and NaOH, and the suspension was kept for 10 min to let the larger particles settle. A 0.01% Au sample with an average size of approximately 12 nm was dropped separately with 0.1% natural and modified sepiolite solutions. After the stirring for 15 min at 400 rpm with an orbital shaker, it was centrifuged at 5000 rpm for 5 min. In here, AuNPs were conditioned to this solution, which is thought to be very dilute and completely dispersed of the sepiolite fibers. The zeta potentials of the supernatant were then measured and recorded. Each data point is an average of approximately twenty measurements, and an average error of these measurements was about ± 2 mV. All measurements were made at ambient temperature (22 ± 1 °C).

2.3. Characterization Analyses

The morphologies and microstructures of natural and modified sepiolite products with CTAB surfactant and AuNPs loading were analyzed by FTIR, environmental scanning electron microscope (ESEM), and TEM in order to determine the change in morphological features of nanoparticle hybrid materials. The Fourier transform IR spectroscopic (FTIR) analyses were conducted on a Perkin-Elmer Spectrum One Fourier Transform spectrometer (Waltham, MA, USA). FTIR studies were performed on natural and modified sepiolite of dried approximately 5 mg samples to explain their chemical properties and functional groups. In order to collect information on the sample's surface and its composition for wet and uncoated electron micrographs of specimens, the environmental scanning electron microscope (ESEM) was used by allowing for a gaseous environment in the specimen chamber. To obtain information on the inner structure of the sample, such as crystal structure, morphology, sizes, and stress state transmittance electron microscopy (TEM) was used. The TEM analyses revealed information about sepiolite loaded with AuNPs. Scanning electron microscopy (ESEM) and transmission electron microscopy (TEM) were used to study the textural features of both natural and modified sepiolite fibers. All samples were first coated with carbon. Using then FEI-Quanta FEG 250 device (Hillsboro, OR, USA), image analysis of all samples was performed in a low vacuum environment and open position ESEM mode. TEM analysis was performed on four samples: natural sepiolite, CTAB/sepiolite, 25 ppm AuNP/sepiolite, and 25 ppm AuNP/CTAB/Sepiolite. The particles were suspended in ethanol for 10 min, and the particles were deposited on carbon film-coated grids. Then, the image analysis was performed. The samples were transferred to the copper grid on the formvar coating without any treatment, and the study was performed. The device was Jeol 2000FX (Tokyo, Japan), and has a lanthanum hexaborate gun.

2.4. Computational Details

In the experimental stage of the study, the adsorption mechanism and capacity of AuNPs onto sepiolite mineral in the presence of CTAB was investigated. Atomic modeling of the subject has also been a subject of curiosity. Therefore, the adsorption of AuNPs on 100 surfaces of sepiolite was simulated in both the presence and absence of CTAB by molecular dynamics techniques. All MD simulations were performed with the Materials Studio 2016 program [35]. First, the crystal data of the sepiolite unit cell was taken from the American Mineralogist Crystal Structure database [36]. The cell was then enlarged $2 \times 2 \times 6$ times and rebuilt along 100 surfaces to yield a supercell of $200 \text{ \AA} \times 54.10 \text{ \AA} \times 31.62 \text{ \AA}$. All dangling bonds and atoms in the obtained cell were saturated with hydrogen. CTAB molecule was then plotted using the same program. The pure gold metal cell was also taken into the library of the program and expanded $2 \times 2 \times 2$ times to produce an AuNP including 24 atoms.

Five models were developed based on experimental studies. Those consist of AuNPs/SEP, monolayer CTAB/SEP, bilayer CTAB/SEP, and the last two were constructed by placing AuNPs between CTAB and sepiolite interface separately. Initial supercells were given in Figure 1.

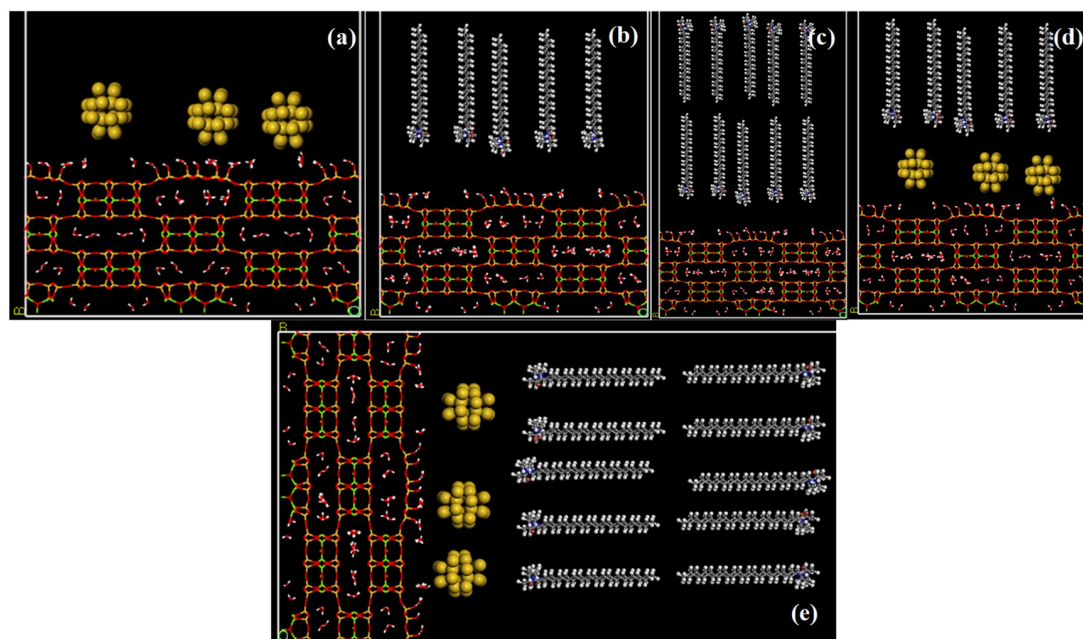


Figure 1. Initial structures of models: gold nanoparticles/sepiolite (AuNPs/SEP) (a), monolayer CTAB/SEP (b), bilayer CTAB/SEP (c), monolayer AuNPs/SEP (d), and bilayer AuNPs/SEP (e). Red, white, yellow, green, cream yellow, baroque red, blue, and gray represent oxygen, hydrogen, gold, magnesium, silicon, nitrogen, and bromine and carbon atoms, respectively.

The periodic supercell structures given in Figure 1 are the initial geometry for MD simulations. The gap to get rid of the interaction of the upper periodic image, which is 200 Å for molecules to move freely, was not shown for clear visibility of molecules. The line style structure consisting of channels and tunnels was the sepiolite mineral. Structural zeolitic and crystal waters were seen in the tunnels. Yellow and CPK-style nanoparticles represent AuNPs. Ball and stick-like structures consisting of hydrophobic aliphatic chains ($-\text{CH}_2$) and hydrophilic heads ($-\text{N}-\text{CH}_3$) are CTAB molecules. Those molecules were placed on the sepiolite surface in the form of monolayer (Figure 1b,d) and bilayer (Figure 1c,e) to reveal the adsorption capacity and mechanism of the gold nanoparticles. The monolayer coating was formed by adding 15 CTAB molecules on average considering the total basal surface area of sepiolite. The bilayer formation was formed by twice this.

Simulations and geometry optimization were performed with the Forcite module of MS 2016 program [35]. Before starting geometry optimization, the total net charge was introduced to zero with the consistent-valence force field (CVFF) [37] parameters. Hydrogen charge of the water molecules in the models was appointed as +0.41, oxygen as −0.82, and the charge for bromine ion as −1 and thus total charge was zero. All of the atoms in the models were in the mobile position to understand the interaction of the gold nanoparticles with the surfactants and sepiolite. For the geometry optimization, 5000 iterations steepest descent, and 1000 iterations conjugate gradient algorithms were used. The aim of geometry optimization is to introduce the force field parameters to all atoms in the models and to avoid possible irregularities. The convergence criteria were for energy 0.001 kcal/mol and for force 0.5 kcal/mol/Å. Long-range columbic interactions were calculated using the Ewald summation method. The repulsive cutoff is 12 Å for the van der Waals term. Ewald was used as the summation method for both electrostatic and van der Waals terms. In the simulation stage, the above optimization parameters were used exactly and the time step was taken as 1 femtosecond (fs). The equilibration simulation ran as 250 picoseconds (ps) with the constant volume and temperature ensemble (NVT) while the production

simulation lasted with the constant pressure and temperature ensemble (NPT) as 1 nanosecond (ns). All simulations were carried out at 298 K and the temperature and pressure was controlled by the Nose thermostat [38] and Berendsen barostat [39], respectively. All those optimization and simulation parameters and steps have been used successfully in recent studies [25,40–45].

The interaction energies were calculated as a result of the simulations to determine the amount of adsorption and the effective force causing it. Interaction energies were automatically calculated by the scripting file in Materials Studio [35] with the help of the following generic formula:

$$E_{IE} = E_{TOTAL} - (E_{FRAGMENT1} + E_{FRAGMENT2}) \quad (1)$$

Here, E_{IE} represents the interaction energy (IE) of the considered systems, E_{TOTAL} is the total energy of the whole system, and $E_{FRAGMENT1}$ and $E_{FRAGMENT2}$ represent the energies of the monomers, respectively.

3. Results and Discussion

3.1. Experimental Studies

The zeta potentials of AuNPs, and natural and modified sepiolite samples are shown in Figure 2. As seen from Figure 2 that while a zero point of charge (zpc) of natural sepiolite was obtained around pH 3.2, the AuNPs showed negative charges at all pH values. On the other hand, in the sepiolite sample modified with CTAB, the surface was completely positive. It can be said that the entire surface of the sepiolite was adsorbed with CTAB. Li et al. reported that pure sepiolite features totally negative surfaces in all pH but after organically modified with CTAB, organo-sepiolite hybrids show positive zeta potential especially before natural pH [46]. To explain the charge distribution of AuNPs on natural sepiolite (NS) and modified sepiolite (MS) surfaces, zeta potential curves of the samples are given in Figure 3.

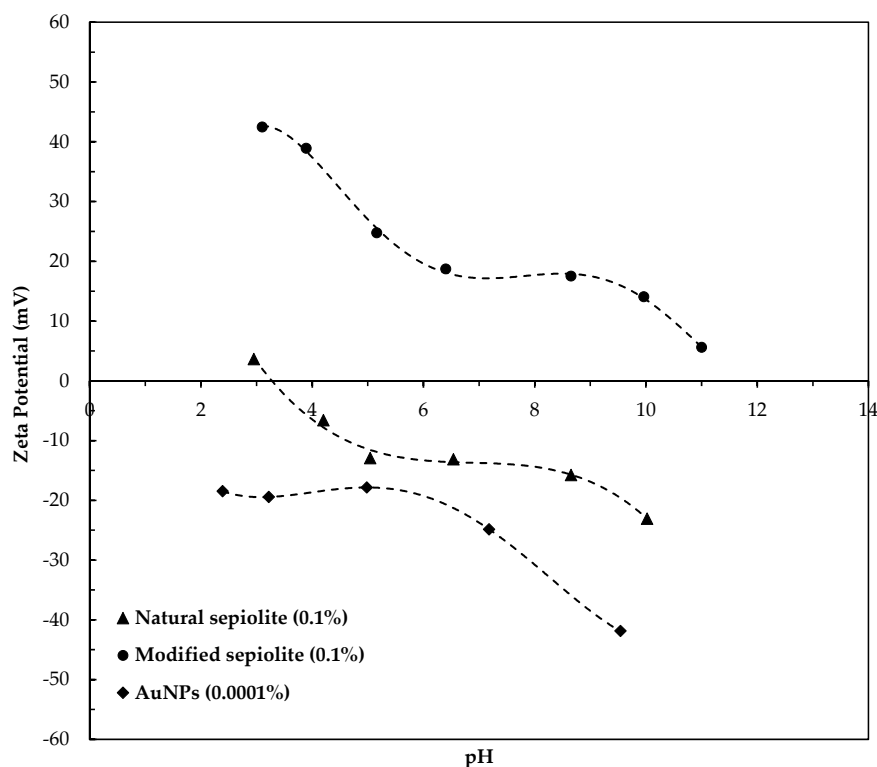


Figure 2. Zeta potentials of natural sepiolite (NS), modified sepiolite (MS), and AuNPs as a function of pH.

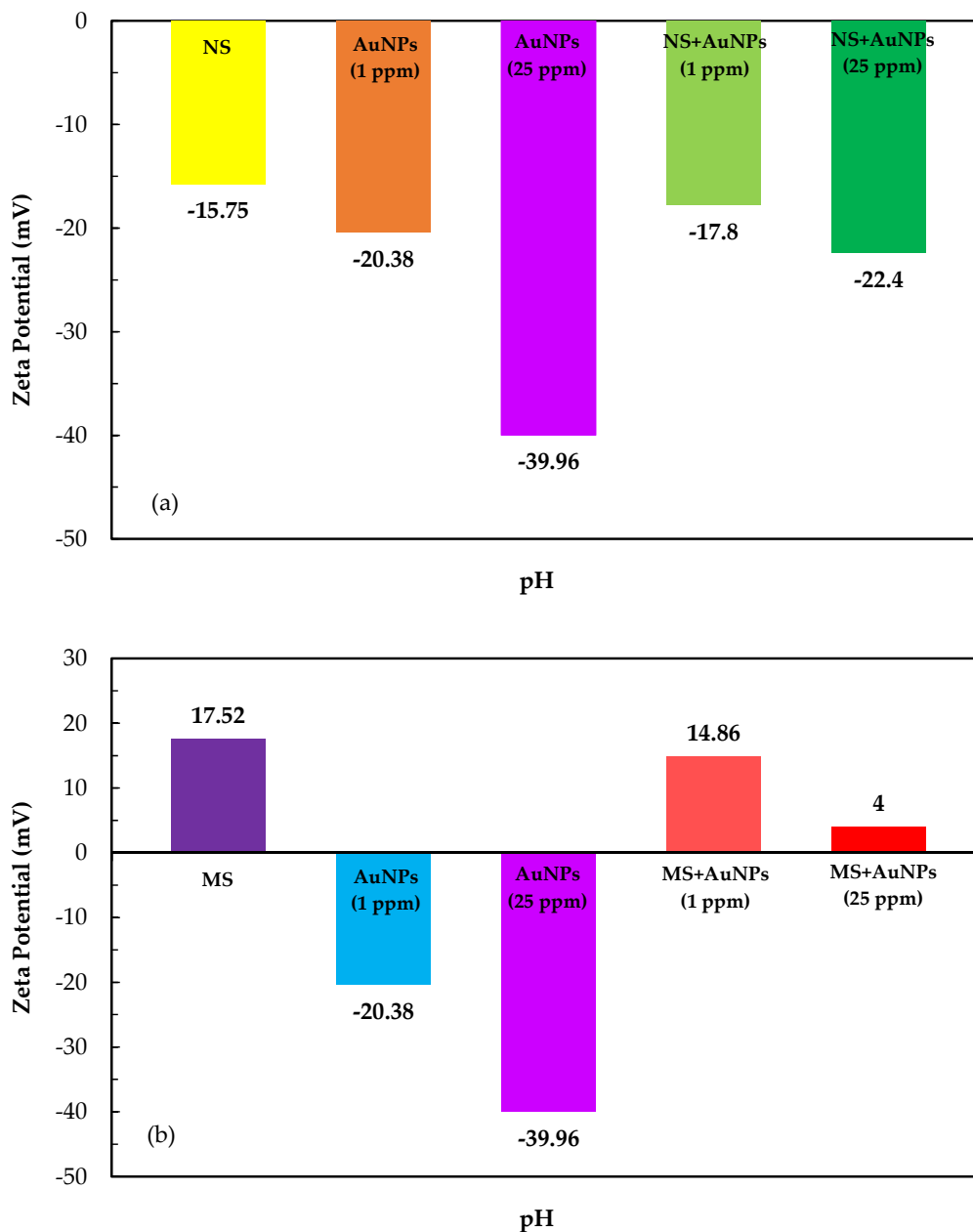


Figure 3. Histograms for zeta potentials of 1 and 25 ppm AuNPs/natural sepiolite (NS) (a) and 1 and 25 ppm AuNPs/modified sepiolite (MS) (b), respectively, as a function of pH.

The zeta potential of 1 and 25 ppm AuNPs yielded -20.38 and -39.86 mV at natural pH, respectively (Figure 3a,b). Interestingly, the 1 and 25 ppm of AuNPs showed no significant coating on the natural sepiolite surfaces, and slightly increased its zeta potential from -15.75 to -17.8 and -22.4 mV, respectively; this can be attributed to both AuNPs and natural sepiolite surfaces carrying negative charges at natural pH. For this reason, the typical cationic surfactant CTAB was used to modify the sepiolite surfaces to increase AuNPs' coating capacity. The results showed that the surface charge of modified sepiolite decreased to $+14.86$ and $+4.01$ mV from $+17.52$ mV upon treating it with 1 and 25 ppm of AuNPs, respectively. It is because a bilayer of CTAB made the CTAB-coated gold nanoparticles positively charged as Sau and Murphy stated [35]. They measured the zeta potential values for CTAB-coated gold nanocrystals in the range $+49$ – $+71$ mV, depending on nanoparticle shape and size. They also added that these zeta potential values hardly changed even after centrifugation and re-dispersion of the nanocrystals in distilled and deionized water, suggesting that the bilayer

structure was quite stable. Therefore, the surface of the nanoparticles was completely positive when gold and CTAB molecules interacted with each other.

Figure 4 shows the schematic illustrations of the interaction of AuNPs with NS and MS surfaces. As seen from Figure 4a, the negatively charged AuNPs partly adsorbed on negatively charged NS surfaces. Since the negative zeta potential of NS particles (-22.4 mV) increased in the presence of AuNPs, the NS particles repelled each other (Figure 4b). The picture seen in Figure 4c also proved that the color of the NS suspension was pinkish indicating that the sizes of AuNPs were about 16 nm. In the case of coating process of AuNPs on MS surfaces, the negatively charged AuNPs significantly adsorbed on the positively charged MS surfaces (Figure 4d). Due to the decrease in the zeta potential of MS particles ($+4$ mV), the MS particles coated with AuNP come closer, and formed aggregates, and the color of the suspension changed to dark blue (Figure 4e). As seen from Figure 4f, the color of MS suspension was dark blue indicating that the sizes of AuNPs were about 150 nm.

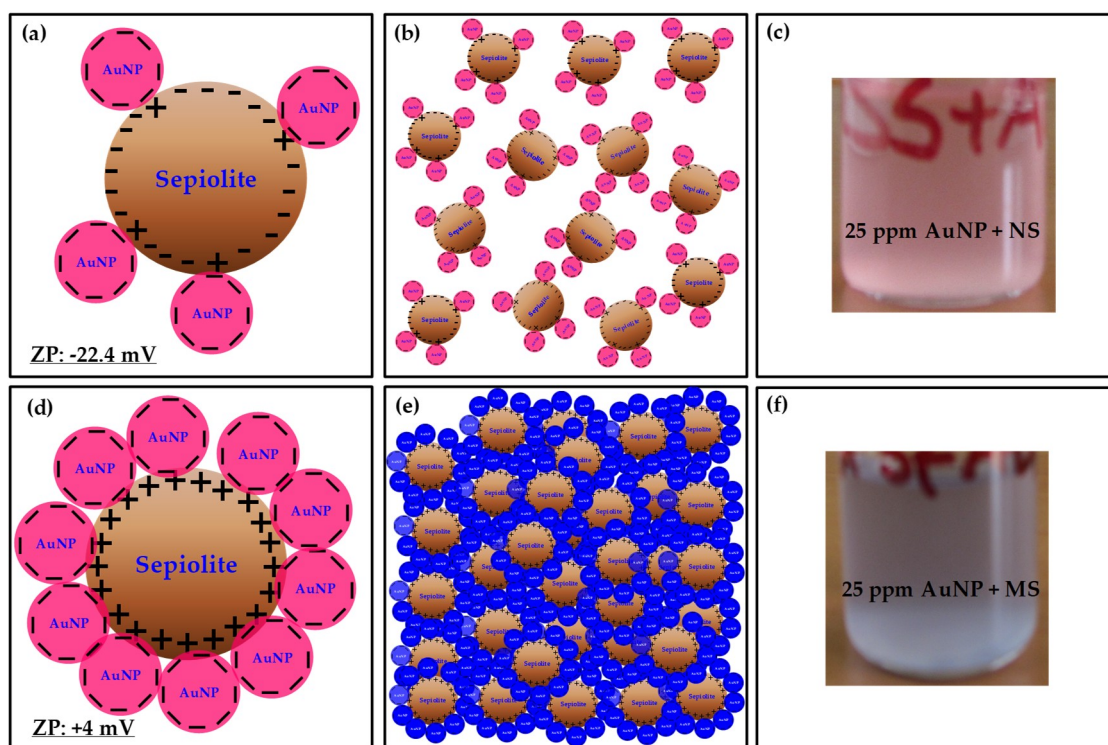


Figure 4. A schematic illustration of the interaction of AuNPs with natural sepiolite (NS) and modified sepiolite (MS). Coating process of AuNPs on NS (a) and MS surfaces (d). AuNPs–NS particles (b) and AuNPs–MS particles (e) in the suspension. Pictures of coating of 25 ppm AuNPs on NS (c) and MS (f) surfaces.

3.2. Characterization Analyses

The FTIR spectra of natural and modified samples were obtained to determine the wavelengths of the modification components on the sepiolite surface of CTAB and to obtain information about adsorption, and the results are shown in Figure 5.

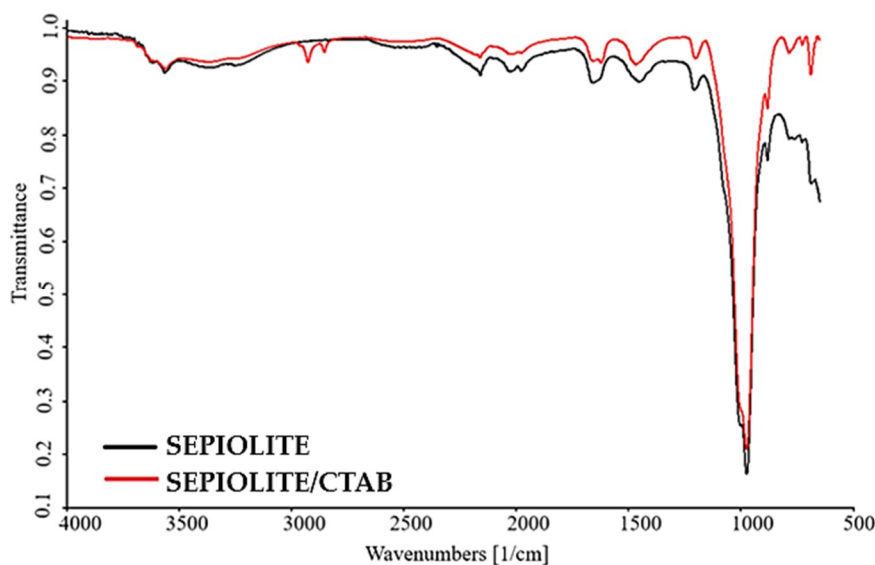


Figure 5. FTIR spectra of natural and modified sepiolite samples.

Characteristic peaks of the natural sepiolite in Figure 5 were the broad band due to the hydroxyl group (-OH) and adsorbed water vibrations in the wavenumber area of $3300\text{--}3500\text{ cm}^{-1}$, the vibrations around 2000 and 2200 cm^{-1} were the vibrations caused by carbonated impurities such as calcite and dolomite. The peak at 1650 cm^{-1} was symmetric and asymmetric stretching of the crystal and zeolitic waters, while the peak at 1450 cm^{-1} was known as the carbonate peak. The peaks in the $900\text{--}1000\text{ cm}^{-1}$ region were characterized by silicates (Si-O-Si and Si-O). Peaks in the region of $750\text{--}650\text{ cm}^{-1}$ belonged to magnesium hydroxides. In the peaks of modified sepiolite obtained after treatment with CTAB, shifts to the left around $3\text{--}5\text{ cm}^{-1}$ occurred as a result. Peaks, the most important indicator of CTAB, were the symmetric and asymmetric stretching of -CH_2 and -CH_3 in the region of $2850\text{--}2900\text{ cm}^{-1}$. All of those peaks overlapped with the results obtained from previous studies with sepiolite samples belonging to the same region [47].

ESEM images of natural and modified sepiolite samples were mapped in vacuum mode, and are shown in Figure 6.

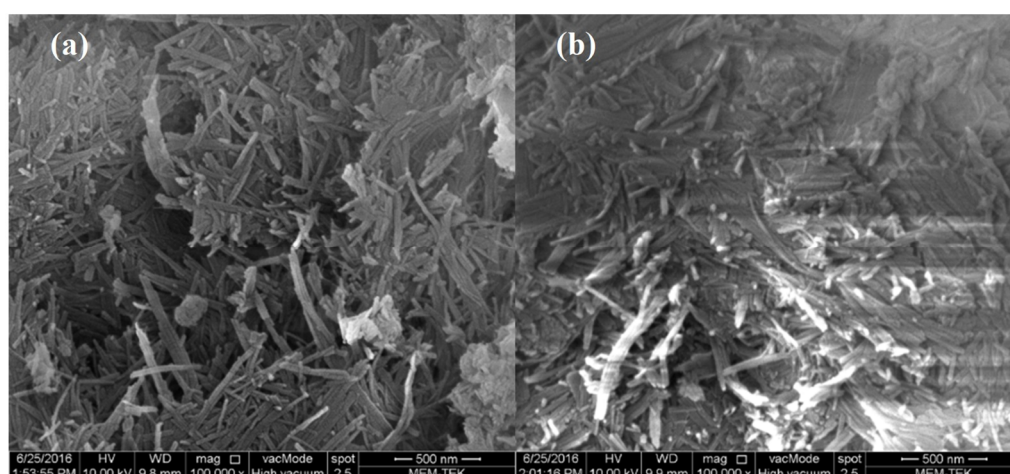


Figure 6. ESEM images for natural (a) and modified (b) sepiolite samples, respectively.

The image of the natural sample in Figure 6a shows the characteristic needle-like fibrous structures of sepiolite. As stated in literature [46], those needle-like fibers connected to each other form dense “packages”. Therefore, it could be observed that natural sepiolite has poor dispersibility due to hydrogen bonding and van der Waals forces that exist among needle-like crystals [46]. Although the

length of the fibers can vary greatly, the width for sepiolite laths and rods were calculated always at nanometric ($\sim 15\text{--}40\text{ nm}$), which is consistent with the observations of literature [48,49]. SEM images of modified sepiolite hybrids (Figure 6b) show that the original morphology and microstructure of sepiolite crystals were preserved intact after modification. The purpose of the modification is to create less dense “packages” and to improve the physico-chemical properties as well as to avoid the collection of fibers [46]. SEM images show that modification with quaternary ammonium salt has a greater effect on the degree of dispersion of the fibers and that quaternary ammonium salts are suitable modifiers to improve the dispersion [46]. After the addition of CTAB, the surfaces of the samples became pale but the fibrosis structures were less stacked on top of each other (Figure 6b). More importantly, the aggregates for natural sepiolite fibers were smoother and more porous and thus it is thought that CTAB molecules could adsorb onto the sepiolite channels and even might enter the tunnels. The images of TEM analysis performed to explain that AuNPs were loaded onto the surfaces of the sepiolite are shown in Figures 7–9. No filtering was performed on the photographs.

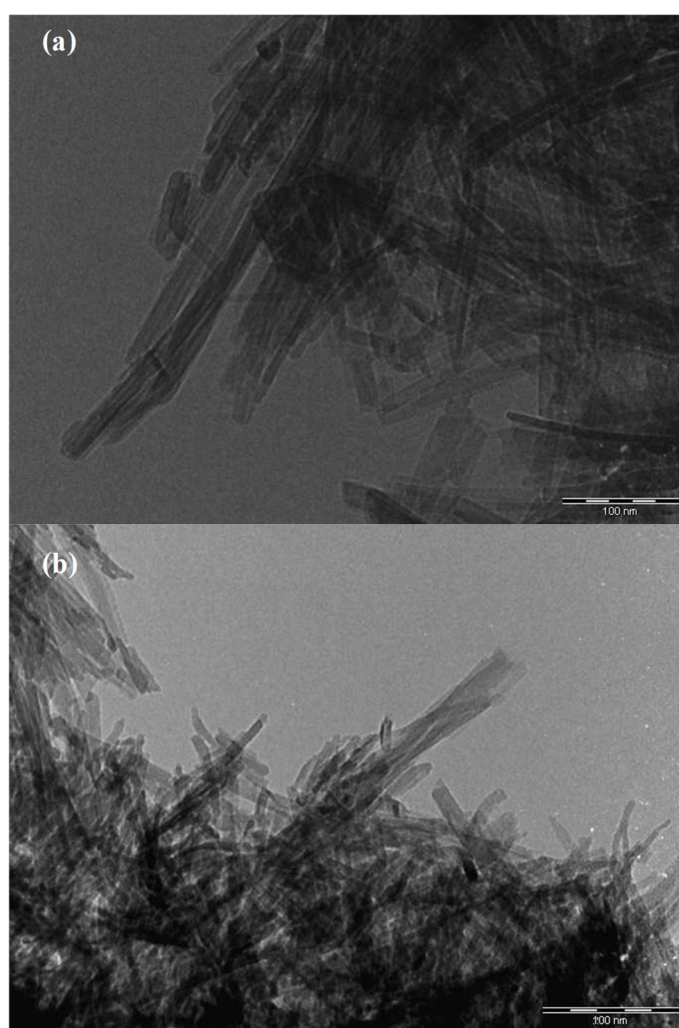


Figure 7. TEM images of natural (a) and modified with CTAB (b) sepiolite, respectively.

What stands out in Figure 7 is that the complexly stacked and fibrous morphological packets in ESEM images appeared in two dimensions with a clean and smooth surface. In a recent study, this unique form of the same sample was discussed and added that the samples of Eskişehir region show their characteristic texture, different from the other sepiolites [50]. After CTAB addition, textural macro porosity occurred due to the aggregation of sepiolite fiber bundles (Figure 7b). TEM analysis results obtained by adding 25 ppm AuNPs to natural sepiolite samples are given in Figure 8.

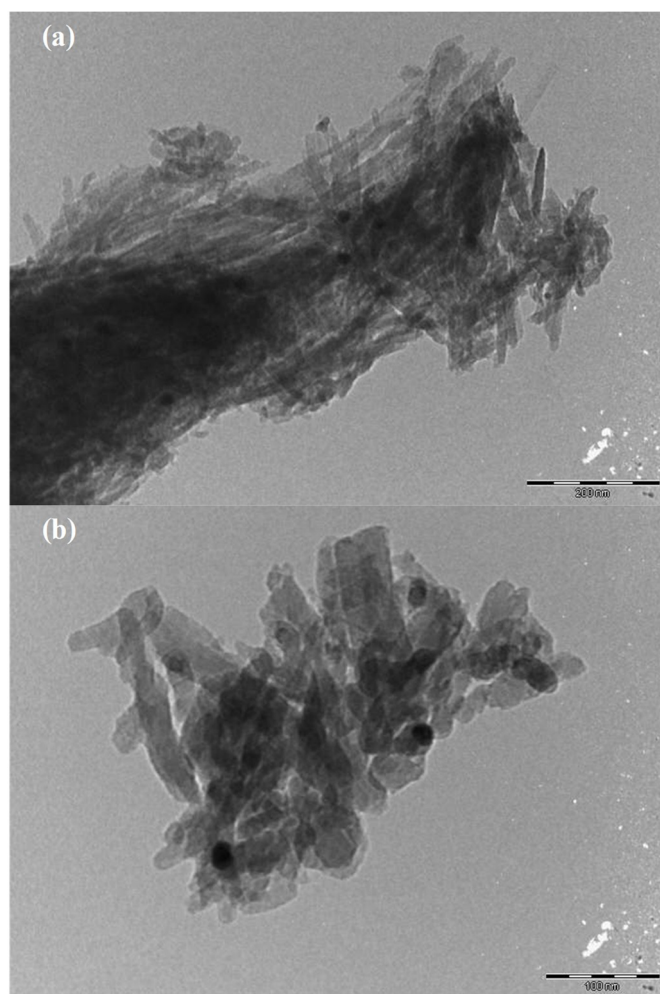


Figure 8. TEM images of 25 ppm AuNPs loaded onto natural sepiolite samples: 200 nm scaled (a) and 100 nm scaled (b), respectively.

The images in Figure 8 show that AuNPs were distributed over natural sepiolite fibers. The average size of these nanoparticles, which were very sparse and small, was about 10 nm. TEM analysis of the samples obtained by adding 25 ppm AuNPs to the modified sepiolite was performed for a better understanding of coating and agglomeration and is given in Figure 9.

AuNPs loaded with modified sepiolite (Figure 9) were more uniform and more than that of natural sepiolite (Figure 8). Furthermore, although theoretically the amount of AuNPs loaded in both samples was the same, those loaded into the modified clay were also larger in average size. Since the average size of the image seen in Figure 8 was around 10 nm but that for Figure 9 was around 20 nm. AuNPs appeared to be distributed regularly on the outer surfaces of the sepiolite. Gold nanoparticles were aligned parallel to the fiber axis (Figure 9). This is thought to be due to the selectivity of the deposition of AuNPs in the regions functionalized by the inoculation of organosilanes previously [20]. Therefore, the regions were expected to be located at the edges of the fibers in regions rich in silanol groups. Similar results and size distributions have been reported in literature [5,20,21].

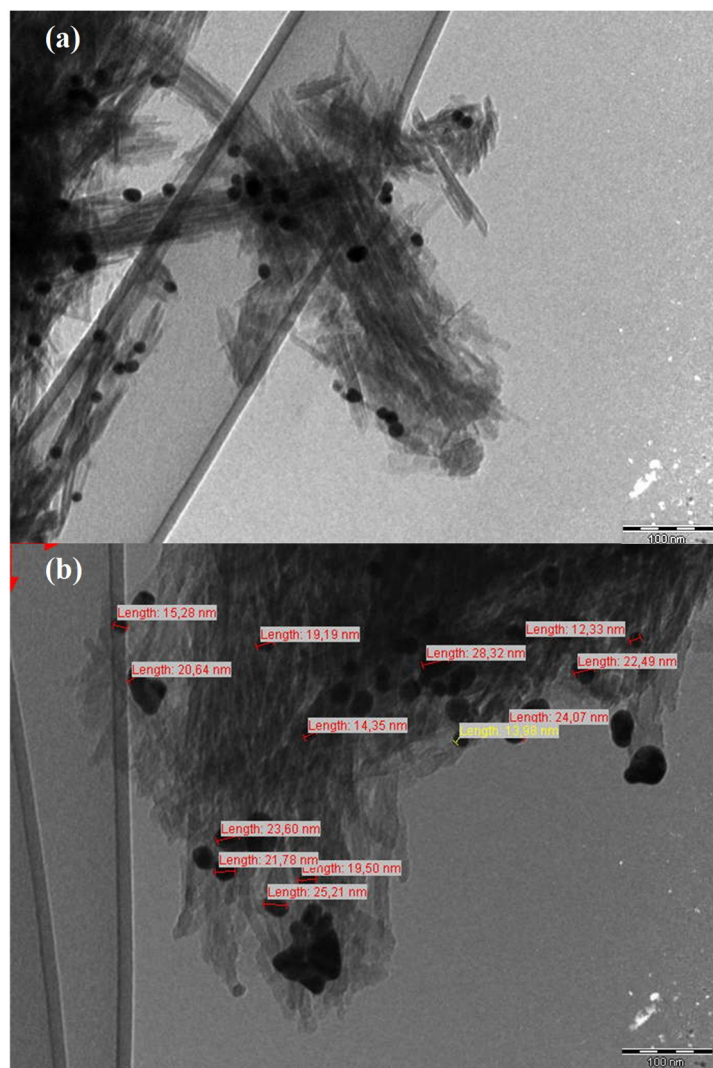


Figure 9. TEM images of 25 ppm AuNPs loaded onto modified sepiolite samples: 200 nm scaled (a) and 100 nm scaled (b), respectively.

3.3. MD Simulations

All the expected states to clarify the coating and formation of AuNPs onto sepiolite basal surface were dynamically simulated. The final structures obtained from the simulations for monolayer and bilayer CTAB/SEP are shown in Figure 10.

The 15 CTAB molecules in the monolayer CTAB/SEP model interacted with $-\text{SiO}$ and $-\text{SiOH}$ groups on the basal surface of the sepiolite due to the large number of H-bonds. It is effective in electrostatic interactions other than those H-bonds indicated by dashed blue lines. Interactions of the water accumulation around the head region of CTAB molecules with the sepiolite surface were neglected. During the simulation, the hydrophilic heads were adsorbed to the hydrophilic surface but the hydrophobic tails walked away from the surface (Figure 10a). On the other hand, the adsorption and distribution of these 15 molecules on the surface was also monitored (Figure 10b). This monolayer adsorption has been frequently mentioned in literature [11,27]. Similar formation changes and interactions were also observed in the bilayer CTAB/SEP model (Figure 10c,d). However, the layer thickness in this model was twice as large. Since the average thicknesses were measured roughly 1 and 2 nm, respectively. In order to explain formation changes and coating in the presence of AuNPs, three AuNPs were added to the models and the simulations were repeated, and the final structures obtained are seen in Figure 11.

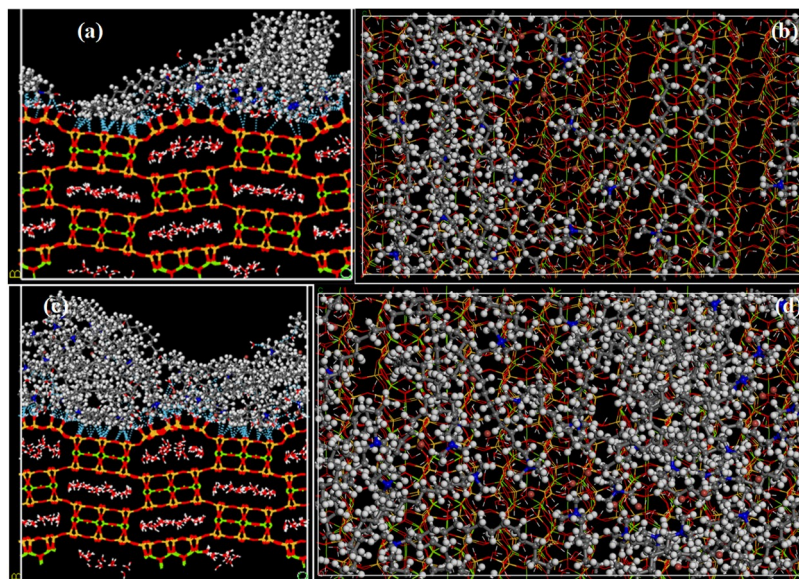


Figure 10. Side (a,c) and top views (b,d) of the final structures for the monolayer CTAB/SEP and bilayer CTAB/SEP models, respectively 1.25 ns later.

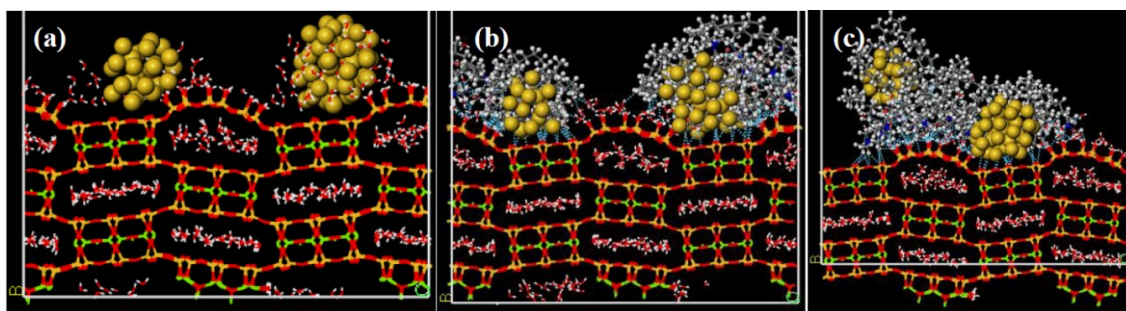


Figure 11. Side views of the final structures for the AuNPs/SEP (a), monolayer AuNPs/SEP (b), and bilayer AuNPs/SEP (c) models, respectively 1.25 ns later.

Throughout the simulation, it was observed that the metal atoms did not break apart from each other and even the median of three AuNPs directed towards the right side one to form a larger nanoparticle due to the electrostatic immobilization of them [51](Figure 11a). In addition, it was also found that the waters in the canals clustered around the hydrophilic gold atoms. In the meantime, $-\text{SiOH}$ groups on the hydrophilic basal surface of the sepiolite were trying not to break with them due to the H-bonds they had made with the water molecules, and thus relatively more bending was observed in the tunnel near the surface. This is a good example of the elasticity in the nature of clays.

The accumulation of gold nanoparticles continued when CTAB was added (Figure 11b,c). In addition, the H-bonds formed in the models in Figure 10 were observed to a lesser extent in these models, especially in the bilayer AuNPs/SEP model. The difference is that in the presence of AuNPs, the CTAB molecules were more rounded and clustered around the gold nanoparticles rather than completely dispersing to the surface. This finding is supported by TEM analyses and literature [20]. On the other hand, the most important difference between the models containing AuNPs was that the small AuNP found in AuNPs/SEP and monolayer AuNPs/SEP models were stabilized in CTAB molecules by moving away from the sepiolite surface in the bilayer AuNPs/SEP model. This is emphasized in literature that CTAB molecules are used to regulate, stabilize particle size, and to adsorb gold nanocrystals in bilayer or multilayer fashion [32]. Another difference is that while all of the CTAB molecules in the monolayer AuNPs/SEP model were adsorbed to the sepiolite surface, half of the CTAB molecules in the bilayer AuNPs/SEP model were deposited on the surface

with gold molecules. The other 15 molecules exceeded 200 Å gap and reached the other basal surface containing magnesium. As a matter of fact, when looking at all three models, it is evident that the tetrahedral-octahedral-tetrahedral sheet at the bottom of the bilayer AuNPs/SEP model had gone too far out of cell. The image of the interaction of the other 15 CTAB molecules with this layer was taken from the periodicity of the cell in Figure 11c (Figure 12). Considering the final structure of all models, it is thought that CTAB molecules tend to adsorb and stabilize around AuNPs as stated in literature [28,30,32].

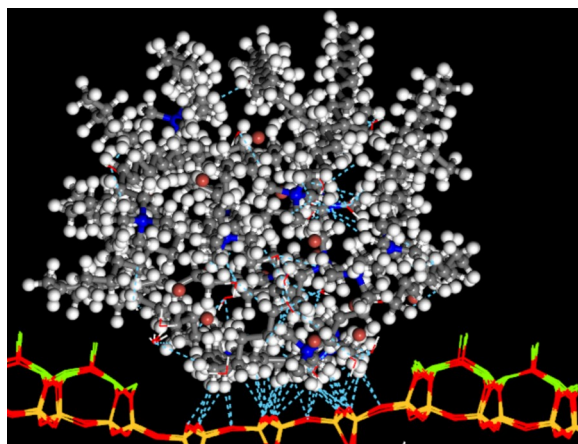


Figure 12. Final snapshot of the severed 15 CTAB molecules on the periodic surface after 1.25 ns.

As the simulation continued, the broken 15 CTAB molecules in the bilayer AuNPs/SEP model first came together as a micelle aggregate. They then collected the water molecules in the sepiolite channel into hydrophilic head regions by H-bond interactions. As a matter of fact, while the hydrophobic tails were facing out, the hydrophilic head groups appeared to be concentrated in the middle region. The discharged channel was filled with those 15 CTAB molecules due to the both H-bonds between oxygen ($-\text{SiO}$) in the tetrahedral layer and hydrogen ($-\text{CH}_2$ and $-\text{CH}_3$) in the surfactant and other electrostatic interactions (Figure 12). Similar interactions and formations have been mentioned in our recent study [8].

In the above models, the interaction energies for AuNPs/SEP, AuNPs/CTAB, and CTAB/SEP pairs were calculated to obtain more information about the components and magnitudes of the mentioned interactions and the results are presented in Table 2. As the interaction energy was calculated, the structural zeolitic and crystal water molecules were taken as if part of sepiolite. Likewise, bromine ions were considered as belonging to CTAB.

Table 2. Interaction energies and its components for each models (kcal/mol).

Pairs	Models	Monolayer CTAB/SEP	Bilayer CTAB/SEP	AuNPs/SEP	Monolayer AuNPs/SEP	Bilayer AuNPs/SEP
AuNPs/SEP	N/A	N/A	N/A	−443.39	−320.28	−242.69
				−443.39 ¹	−320.29 ¹	−242.69 ¹
				0.00 ²	0.00 ²	0.00 ²
AuNPs/CTAB	N/A	N/A	N/A	N/A	−484.26	−526.18
					−484.26 ¹	−526.19 ¹
					0.00 ²	0.00 ²
CTAB/SEP	N/A	−1373.63	−1630.76	N/A	−1011.11	−1575.93
		−99.88 ¹	−126.37 ¹		−83.30 ¹	−125.95 ¹
		−1273.75 ²	−1504.40 ²		−927.81 ²	−1449.98 ²

N/A: not applicable, ¹ and ² colors stands for van der Waals and coulombic energy contributions.

When all interaction energy values were considered, it could be easily said that AuNPs could easily interact with the basal surface of the sepiolite and still strongly interact in the presence of CTAB (Table 2). However, it was observed that the interaction of CTAB/SEP in the models decreased with the addition of AuNPs. The amount of decrease was calculated as 362.52 kcal/mol in monolayer models and 54.83 kcal/mol in the bilayer model. It was thought that the main reason for this was due to the dramatic decrease of the coulombic contribution, although the energy contribution of van der Waals in the monolayer models was slightly reduced. However, it is clear that the effective force between CTAB/SEP was still more coulomb interactions. This result was confirmed by our experimental studies. On the other hand, it is obvious that the parameter affecting the energy changes in AuNPs/SEP and AuNPs/CTAB pairs was van der Waals rather than coulomb interactions. Since the coulomb contribution of these pairs was calculated to be very close to zero. In the presence of CTAB, the AuNPs/SEP interaction decreased by 123.11 and 200.7 kcal/mol in monolayer and bilayer models, respectively. The interaction energy values of AuNPs/CTAB were recorded as −484.26 and −526.16 kcal/mol, respectively. This result is supported by a study with CTAB adsorbed in bilayer formed around gold nanoparticles [28,30,32].

4. Conclusions

In this study, the storage and coating of gold nanoparticles in natural and modified sepiolite samples with high adsorption capacity were demonstrated by experimental and theoretical investigations. The zeta potential measurements were carried out with AuNPs, natural, and modified sepiolite samples. The results indicated that the AuNPs showed no significant coating on the natural sepiolite surfaces because both AuNPs and natural sepiolite surfaces carry negative charges at natural pH. The typical cationic surfactant, CTAB, was used to modify the sepiolite surfaces to increase AuNPs' coating capacity. The modification of sepiolite with amine molecules made it positively charged, and in turn considerably increased the AuNPs coating on sepiolite surfaces due to electrostatic attraction. The characterization tests of the samples showed that AuNPs were deposited along the fibers of the sepiolite and their dimensions were measured as an average of 20 nm. The adsorption mechanism and coating of AuNPs were modeled by MD simulations. In these simulations, it was found that AuNPs deposited in the channels of sepiolite in the basal surfaces of the sepiolite both in the presence and absence of CTAB, and the effective forces that provided this were van der Waals and H-bond interactions. In models with CTAB, AuNPs had decorated the surface of the sepiolite, but the driving force for the CTAB/SEP pair was coulombic interactions. The results obtained from this study were discussed with literature experimentally and theoretically. Finally, it could be concluded that the sepiolite particles coated with AuNPs are considered as excellent water-processable materials.

Author Contributions: Experimental methodology, O.O. and D.S.A.; software, D.K.; validation, O.O., I.K.U. and D.K.; formal analysis, O.O.; investigation, D.S.A. and D.K.; resources, D.K.; data curation, D.K.; writing—original draft preparation, D.K. and D.S.A.; writing—review and editing, D.K. and O.O.; visualization, D.K. and O.O.; supervision, O.O.; project administration, D.K. and O.O.

Funding: This research received no external funding.

Acknowledgments: This work was supported by Scientific Research Projects Coordination Unit of Istanbul University-Cerrahpasa, Project number 42265. Computing resources for computational studies used in this work were provided by the National Centre for High Performance Computing of Turkey (UYBHM) under grant number 5003682015.

Conflicts of Interest: The authors declare no conflict of interest.

References

1. Newman, J.D.; Blanchard, G.J. Formation of gold nanoparticles using amine reducing agents. *Langmuir* **2006**, *22*, 5882–5887. [[CrossRef](#)] [[PubMed](#)]

2. Pecharromán, C.; Esteban-Cubillo, A.; Fernández, H.; Esteban-Tejeda, L.; Pina-Zapardiel, R.; Moya, J.S.; Solis, J.; Afonso, C.N. Synthesis, conforming, linear, and non-linear optical properties of gold nanoparticles-sepiolite compacts. *Plasmonics* **2009**, *4*, 261–266. [[CrossRef](#)]
3. Tiwari, N.; Kalele, S.; Kulkarni, S.K. Modulation of optical properties of gold nanorods on addition of KOH. *Plasmonics* **2007**, *2*, 231–236. [[CrossRef](#)]
4. Zhang, R.; Hummelgard, M.; Olin, H. Simple synthesis of clay-gold nanocomposites with tunable color. *Langmuir* **2010**, *26*, 5823–5828. [[CrossRef](#)] [[PubMed](#)]
5. Zhu, L.; Letaief, S.; Liu, Y.; Gervais, F.; Detellier, C. Clay mineral-supported gold nanoparticles. *Appl. Clay Sci.* **2009**, *43*, 439–446. [[CrossRef](#)]
6. Ung, T.; Liz-Marzán, L.M.; Mulvaney, P. Optical properties of thin films of Au@SiO₂ particles. *J. Phys. Chem. B* **2001**, *105*, 3441–3452. [[CrossRef](#)]
7. Kelly, K.L.; Coronado, E.; Zhao, L.L.; Schatz, G.C. The optical properties of metal nanoparticles: The influence of size, shape, and dielectric environment. *J. Phys. Chem. B* **2003**, *107*, 668–677. [[CrossRef](#)]
8. Karataş, D.; Senol-Arslan, D.; Ozdemir, O. Experimental and atomistic modeling of adsorption of azo acid 57 on sepiolite. *Clays Clay Miner.* **2018**. [[CrossRef](#)]
9. Ozdemir, O.; Armagan, B.; Turan, M.; Çelik, M.S. Comparison of the adsorption characteristics of azo-reactive dyes on mesoporous minerals. *Dye. Pigment.* **2004**, *62*, 49–60. [[CrossRef](#)]
10. Ozdemir, O.; Cinar, M.; Sabah, E.; Arslan, F.; Celik, M.S. Adsorption of anionic surfactants onto sepiolite. *J. Hazard. Mater.* **2007**, *147*, 625–632. [[CrossRef](#)]
11. Sabah, E.; Çelik, M.S. Adsorption mechanism of quaternary amines by sepiolite. *Sep. Sci. Technol.* **2002**, *37*, 3081–3097. [[CrossRef](#)]
12. Sabah, E.; Çinar, M.; Çelik, M.S. Decolorization of vegetable oils: Adsorption mechanism of β -carotene on acid-activated sepiolite. *Food Chem.* **2007**, *100*, 1661–1668. [[CrossRef](#)]
13. Belova, V.; Andreeva, D.V.; Möhwald, H.; Shchukin, D.G. Ultrasonic intercalation of gold nanoparticles into clay matrix in the presence of surface-active materials. Part I: Neutral polyethylene glycol. *J. Phys. Chem. C* **2009**, *113*, 5381–5389. [[CrossRef](#)]
14. Belova, V.; Möhwald, H.; Shchukin, D.G. Ultrasonic intercalation of gold nanoparticles into a clay matrix in the presence of surface-active materials. Part II: Negative sodium dodecylsulfate and positive cetyltrimethylammonium bromide. *J. Phys. Chem. C* **2009**, *113*, 6751–6760. [[CrossRef](#)]
15. Chenouf, M.; Megías-Sayago, C.; Ammari, F.; Ivanova, S.; Centeno, M.; Odriozola, J. Immobilization of stabilized gold nanoparticles on various ceria-based oxides: Influence of the protecting agent on the glucose oxidation reaction. *Catalysts* **2019**, *9*, 125. [[CrossRef](#)]
16. Yadav, D.K.; Gupta, R.; Ganesan, V.; Sonkar, P.K. Individual and simultaneous voltammetric determination of ascorbic acid, uric acid and folic acid by using a glassy carbon electrode modified with gold nanoparticles linked to bentonite via cysteine groups. *Microchim. Acta* **2017**, *184*, 1951–1957. [[CrossRef](#)]
17. Letaief, S.; Pell, W.; Detellier, C. Deposition of gold nanoparticles on organo-kaolinite—Application in electrocatalysis for carbon monoxide oxidation. *Can. J. Chem.* **2011**, *89*, 845–853. [[CrossRef](#)]
18. Philip, A.; Lihavainen, J.; Keinänen, M.; Pakkanen, T.T. Gold nanoparticle-decorated halloysite nanotubes—Selective catalysts for benzyl alcohol oxidation. *Appl. Clay Sci.* **2017**, *143*, 80–88. [[CrossRef](#)]
19. Mukhopadhyay, K.; Phadtare, S.; Vinod, V.P.; Kumar, A.; Rao, M.; Chaudhari, R.V.; Sastry, M. Gold nanoparticles assembled on amine-functionalized Na–Y zeolite: A biocompatible surface for enzyme immobilization. *Langmuir* **2003**, *19*, 3858–3863. [[CrossRef](#)]
20. Letaief, S.; Grant, S.; Detellier, C. Phenol acetylation under mild conditions catalyzed by gold nanoparticles supported on functional pre-acidified sepiolite. *Appl. Clay Sci.* **2011**, *53*, 236–243. [[CrossRef](#)]
21. Pecharromán, C.; Esteban-Cubillo, A.; Montero, I.; Moya, J.S.; Aguilar, E.; Santarén, J.; Alvarez, A. Monodisperse and corrosion-resistant metallic nanoparticles embedded into sepiolite particles for optical and magnetic applications. *J. Am. Ceram. Soc.* **2006**, *89*, 3043–3049. [[CrossRef](#)]
22. Tiemblo, P.; Benito, E.; García, N.; Esteban-Cubillo, A.; Pina-Zapardiel, R.; Pecharromán, C. Multiscale gold and silver plasmonic plastics by melt compounding. *RSC Adv.* **2012**, *2*, 915–919. [[CrossRef](#)]
23. Liu, M.; Pu, M.; Ma, H. Preparation, structure and thermal properties of polylactide/sepiolite nanocomposites with and without organic modifiers. *Compos. Sci. Technol.* **2012**, *72*, 1508–1514. [[CrossRef](#)]

24. Ma, Y.; Wu, X.; Zhang, G. Core-shell Ag@Pt nanoparticles supported on sepiolite nanofibers for the catalytic reduction of nitrophenols in water: Enhanced catalytic performance and DFT study. *Appl. Catal. B: Environ.* **2017**, *205*, 262–270. [[CrossRef](#)]
25. Rebitski, E.P.; Alcântara, A.C.S.; Darder, M.; Cansian, R.L.; Gómez-Hortigüela, L.; Pergher, S.B.C. Functional carboxymethylcellulose/zein bionanocomposite films based on neomycin supported on sepiolite or montmorillonite clays. *ACS Omega* **2018**, *3*, 13538–13550. [[CrossRef](#)]
26. Fitaroni, L.B.; Venâncio, T.; Tanaka, F.H.; Gimenez, J.C.F.; Costa, J.A.S.; Cruz, S.A. Organically modified sepiolite: Thermal treatment and chemical and morphological properties. *Appl. Clay Sci.* **2019**, *179*, 105149. [[CrossRef](#)]
27. Sabah, E.; Turan, M.; Çelik, M.S. Adsorption mechanism of cationic surfactants onto acid- and heat-activated sepiolites. *Water Res.* **2002**, *36*, 3957–3964. [[CrossRef](#)]
28. da Silva, J.; Dias, R.; da Hora, G.; Soares, T.; Meneghetti, M. Molecular dynamics simulations of cetyltrimethylammonium bromide (CTAB) micelles and their interactions with a gold surface in aqueous solution. *J. Braz. Chem. Soc.* **2017**. [[CrossRef](#)]
29. de Barros, H.R.; Piován, L.; Sassaki, G.L.; de Araujo Sabry, D.; Mattoso, N.; Nunes, A.M.; Meneghetti, M.R.; Riegel-Vidotti, I.C. Surface interactions of gold nanorods and polysaccharides: From clusters to individual nanoparticles. *Carbohydr. Polym.* **2016**, *152*, 479–486. [[CrossRef](#)]
30. Meena, S.K.; Celiksoy, S.; Schafer, P.; Henkel, A.; Sonnichsen, C.; Sulpizi, M. The role of halide ions in the anisotropic growth of gold nanoparticles: A microscopic, atomistic perspective. *Phys. Chem. Chem. Phys.* **2016**, *18*, 13246–13254. [[CrossRef](#)]
31. Meena, S.K.; Sulpizi, M. Understanding the microscopic origin of gold nanoparticle anisotropic growth from molecular dynamics simulations. *Langmuir* **2013**, *29*, 14954–14961. [[CrossRef](#)] [[PubMed](#)]
32. Sau, T.K.; Murphy, C.J. Self-assembly patterns formed upon solvent evaporation of aqueous cetyltrimethylammonium bromide-coated gold nanoparticles of various shapes. *Langmuir* **2005**, *21*, 2923–2929. [[CrossRef](#)] [[PubMed](#)]
33. Frens, G. Controlled nucleation for the regulation of the particle size in monodisperse gold suspensions. *Nat. Phys. Sci.* **1973**, *241*, 20–22. [[CrossRef](#)]
34. Armagan, B.; Ozdemir, O.; Turan, M.; Celik, M.S. Adsorption of negatively charged azo dyes onto surfactant-modified sepiolite. *J. Environ. Eng.* **2003**, *129*, 709–715. [[CrossRef](#)]
35. Dassault Systèmes BIOVIA. *Materials Studio*. 16.1.0.21; Dassault Systèmes BIOVIA: San Diego, CA, USA, 2016.
36. Post, J.E.; Bish, D.L.; Heaney, P.J. Synchrotron powder X-ray diffraction study of the structure and dehydration behavior of sepiolite. *Am. Mineral.* **2007**, *92*, 91–97. [[CrossRef](#)]
37. Dauber-Osguthorpe, P.; Roberts, V.A.; Osguthorpe, D.J.; Wolff, J.; Genest, M.; Hagler, A.T. Structure and energetics of ligand binding to proteins: Escherichia coli dihydrofolate reductase-trimethoprim, a drug-receptor system. *Proteins* **1988**, *4*, 31–47. [[CrossRef](#)]
38. Nosé, S. A unified formulation of the constant temperature molecular dynamics methods. *J. Chem. Phys.* **1984**, *81*, 511–519. [[CrossRef](#)]
39. Berendsen, H.J.C.; Postma, J.P.M.; van Gunsteren, W.F.; DiNola, A.; Haak, J.R. Molecular dynamics with coupling to an external bath. *J. Chem. Phys.* **1984**, *81*, 3684–3690. [[CrossRef](#)]
40. Jaishankar, A.; Jusufi, A.; Vreeland, J.L.; Deighton, S.; Pelletiere, J.; Schilowitz, A.M. Adsorption of stearic acid at the iron oxide/oil interface: Theory, experiments, and modeling. *Langmuir* **2019**, *35*, 2033–2046. [[CrossRef](#)]
41. Karataş, D.; Tekin, A.; Bahadori, F.; Çelik, M.S. Interaction of curcumin in a drug delivery system including a composite with poly(lactic-co-glycolic acid) and montmorillonite: A density functional theory and molecular dynamics study. *J. Mater. Chem. B* **2017**, *5*, 8070–8082. [[CrossRef](#)]
42. Li, J.-W.; Zhang, S.-H.; Gou, R.-J.; Han, G.; Chen, M.-H. The effect of crystal-solvent interaction on crystal growth and morphology. *J. Cryst. Growth* **2019**, *507*, 260–269. [[CrossRef](#)]
43. Li, W.; Pang, X.; Snape, C.; Zhang, B.; Zheng, D.; Zhang, X. Molecular simulation study on methane adsorption capacity and mechanism in clay minerals: Effect of clay type, pressure, and water saturation in shales. *Energy Fuels* **2019**, *33*, 765–778. [[CrossRef](#)]
44. Rahmani, F.; Nouranian, S. Thermal analysis of montmorillonite/graphene double-layer coating as a potential lightning strike protective layer for cross-linked epoxy by molecular dynamics simulation. *ACS Appl. Nano Mater.* **2018**, *1*, 2521–2525. [[CrossRef](#)]

45. Yamamoto, K.; Kawaguchi, D.; Sasahara, K.; Inutsuka, M.; Yamamoto, S.; Uchida, K.; Mita, K.; Ogawa, H.; Takenaka, M.; Tanaka, K. Aggregation states of poly(4-methylpentene-1) at a solid interface. *Polym. J.* **2018**, *51*, 247–255. [[CrossRef](#)]
46. Li, Y.; Wang, M.; Sun, D.; Li, Y.; Wu, T. Effective removal of emulsified oil from oily wastewater using surfactant-modified sepiolite. *Appl. Clay Sci.* **2018**, *157*, 227–236. [[CrossRef](#)]
47. Karataş, D.; Tekin, A.; Çelik, M.S. Adsorption of quaternary amine surfactants and their penetration into the intracrystalline cavities of sepiolite. *New J. Chem.* **2013**, *37*, 3936. [[CrossRef](#)]
48. Garcia-Romero, E.; Suarez, M. Sepiolite-palygorskite polysomatic series: Oriented aggregation as a crystal growth mechanism in natural environments. *Am. Mineral.* **2014**, *99*, 1653–1661. [[CrossRef](#)]
49. Vivaldi, J.L.M.; Robertson, R. Palygorskite and sepiolite (the hormites). In *The Electron-Optical Investigation of Clays*; Gard, J.A., Ed.; The Mineralogical Society: London, UK, 1971; Volume 41, pp. 255–257.
50. Suárez, M.; García-Romero, E. Variability of the surface properties of sepiolite. *Appl. Clay Sci.* **2012**, *67–68*, 72–82. [[CrossRef](#)]
51. Sastry, M.; Rao, M.; Ganesh, K.N. Electrostatic assembly of nanoparticles and biomacromolecules. *Acc. Chem. Res.* **2002**, *35*, 847–855. [[CrossRef](#)]



© 2019 by the authors. Licensee MDPI, Basel, Switzerland. This article is an open access article distributed under the terms and conditions of the Creative Commons Attribution (CC BY) license (<http://creativecommons.org/licenses/by/4.0/>).